Alkanethiol Molecules Containing an Aromatic Moiety Self-Assembled onto Gold Clusters

ARTICLE *in* LANGMUIR · JANUARY 1997

Impact Factor: 4.46 · DOI: 10.1021/la9607520

4 AUTHORS, INCLUDING:

Stephen D Evans
University of Leeds
227 PUBLICATIONS **6,250** CITATIONS

SEE PROFILE

Alkanethiol Molecules Containing an Aromatic Moiety Self-Assembled onto Gold Clusters

S. R. Johnson,† S. D. Evans,*,† S. W. Mahon,‡ and A. Ulman§

Department of Physics and Astronomy and School of Materials, Leeds University, Leeds LS2 9JT, U.K., and Department of Chemistry, The Polytechnic University of Brooklyn, Brooklyn, New York

Received July 30, 1996⊗

Alkanethiol molecules containing a polar aromatic group ($C_{22}H_{45}-SO_2-C_6H_4-O-C_4H_8-SH$) were used to stabilize gold clusters, formed in a two-phase system (*J. Chem. Soc., Chem. Commun.* **1994**, 801). The gold nanoparticles were investigated using TEM, FTIR, UV/vis and X-ray photoelectron spectroscopy and compared to a monolayer formed from the same alkanelthiol molecule onto a planar surface. The results show that surfactant-coated nanoparticles are indeed formed and that the incorporation of a polar aromatic group, into the thiol molecule, does not hinder the self-assembling process.

Introduction

There is currently great interest in the formation of metallic and semiconducting nanoparticles.[2,3] This stems from the fact that their physical properties are dependent on their size, shape, and packing density and leads them to exhibit properties which are different from those of the bulk material.[4−6] For example, bulk gold is metallic in nature while colloidal gold nanoparticles with radii in the range 1−2 nm have electronic properties which fall somewhere between those of metals and semiconductors. Such nanoparticle systems may possibly find applications in many diverse areas of technology including optoelectronics, chemical and biosensors, drug delivery, and catalysis.[7]

Gold nanoparticles have been found to be particularly useful for cell labeling in biology and the formation of reproducible surfaces for surface-enhanced raman scattering.[8] Our interest lies in the physical properties of films formed from such nanoparticles, in particular in their electronic and optical properties. In this regard we are interested in the effects of using surfactants containing large dipole moments to stabilize the nanoparticles. The net perpendicular component of the dipole is expected to alter the electronic and optical (both linear and nonlinear) properties of such films. This initial investigation focuses on the structural characterization and shows that the use of such alkanethiol derivatives to form ligand-stabilized nanoparticles is possible.

There are various methods for synthesizing metallic nanoparticles, ranging in size from 1 to 100 nm, including the use of reverse micelles as reaction vessels in which the size of the nanoparticles is determined by the water content of the vesicle[9] and the classic citrate method for the generation of gold colloids.[10] These techniques, however, suffer serious drawbacks, namely that the nanoparticles made under these conditions are prone to aggregation if the reaction conditions are not carefully controlled, i.e. revert back to the bulk product. Further, the experimental procedures outlined above involve too many variables; e.g., for the citrate method changes in particle size and shape are dependent on the type of reducing agent and the concentration and pH of the reagents. New routes for preparation of nanoparticles which are resistant to aggregation and are easily synthesized are therefore desirable. Recent work by Brust *et al.* has shown that this can be achieved by using surfactants, where the surfactants not only impart stability to the clusters but also define the reactivity and solubility of the nanoparticles.[11]

The method followed in this paper is a modified version of the experimental synthesis first reported by Brust *et al.*, and subsequently followed by Leff *et al.*, which involves the nanoparticles being thermodynamically stabilized by the presence of surfactant molecules.[1,12] According to Leff *et al.*, since the formation of gold nanoparticles is thermodynamically favorable, the gold/solution interfacial energy is lowered by the chemisorption of a thiol monolayer onto the surface of the gold nanoparticle and the nanoparticle bond energy is offset by the enhanced thiol−thiol dispersion attractions.[12]

To date relatively simple "straight alkyl chain" surfactants have been used to stabilize such gold nanoparticles; in this report we show that molecules containing polar, aromatic groups may be used.[13−16] The ability to place "polar" groups onto the surface is of interest for NLO applications, particularly electro-optical and χ^3 effects,

* To whom correspondence should be addressed.
† Department of Physics and Astronomy, Leeds University.
‡ School of Materials, Leeds University.
§ Department of Chemistry, The Polytechnic University of Brooklyn.
⊗ Abstract published in *Advance ACS Abstracts,* December 15, 1996.

(1) Brust, M.; Walker, M.; Bethell, D.; Schiffrin, D. J.; Whyman, R. *J. Chem. Soc., Chem. Commun.* **1994**, 801.
(2) Schmid, G. *Clusters and Colloids. From Theory to Applications*; VCH: New York, 1994.
(3) Alivisatos, A. P. *Science.* **1996**, *271*, 933.
(4) Bawendi, M.; Stierderwald, M. L.; Brus, L. E. *Annu. Rev. Phys. Chem.* **1990**, *4*, 477.
(5) Wang, Y.; Herron, N. J. *J. Phys. Chem.* **1991**, *95*, 525.
(6) Siegel, R. *Nanostructured Mater.* **1993**, *3*, 1.
(7) Hoffman, A. J.; Mills, G.; Yee, H.; Hoffman, M. R. *J. Phys. Chem.* **1992**, *96*, 5546.
(8) Freeman, R. G.; Grabar, K. C.; Allison, K. J.; Bright, R. M.; Davis, J. A.; Guthrie, A. P.; Hommer, M. B.; Jackson M. A.; Smith, P. C.; Walter, D. G.; Natan, M. J. *Science* **1995**, *267*, 1629.
(9) Pileni, M. P. *J. Phys. Chem.* **1993**, *97*, 6961.
(10) Frens, G. *Nature (London), Phys. Sci.* **1973**, *241*, 20.
(11) Brust, M.; Fink, J.; Bethell, D.; Schiffrin, D. J.; Kiely, C. *J. Chem. Soc., Chem. Commun.* **1995**, 1655.
(12) Leff, D. V.; Ohara, P. C.; Heath, J. R.; Gelbart, W. M. *J. Phys. Chem.* **1995**, *99*, 7036.
(13) Hosteler, M. J.; Stokes, J. J.; Murray, R. W. *Langmuir.* **1996**, *12*, 3604.
(14) Whetten, R. L.; Khoury, J. T.; Alvarez, M. M.; Murthuy, S.; Vezmar, I.; Wang, Z. L.; Stephens, P. W.; Cleveland, C. L.; Luedtke, W. D.; Landman, U. *Adv. Mater.* **1996**, *8*, 428.
(15) Terrill, R. H.; Postlethwaite, T. A.; Chen, C.; Poon, C.; Terzis, A.; Chen, A.; Hutchinson, J. E.; Clark, M. R.; Wignall, G.; Londono, J. D.; Superfine, R.; Falvo, M.; Johnson, C. S.; Samulski, E. T.; Murray, R. W.; *J. Am Chem. Soc.* **1995**, *117*, 12537.
(16) Badia, A.; Singh, S.; Demers, L.; Cuccia, L.; Brown, G. R.; Lennox, R. B. *Chem. Eur. J.* **1996**, *2*, 359.

S0743-7463(96)00752-4 CCC: $14.00

and for controlling sphere−sphere interactions.[17] For comparative purposes we have formed monolayers on planar substrates.

The ability to form self-assembled monolayers (SAMs) on nanoparticles offers additional practical benefits for monolayer analysis; in particular, the large surface area presented in these systems permits the application of less sensitive, but nonetheless useful, techniques such as NMR, transmission UV/vis, and FTIR.[18]

Experimental Section

Planar Monolayer Preparation. For comparative purposes SAMs were formed directly onto planar gold surfaces, which were prepared by evaporating gold onto glass microscope slides (with a chromium underlayer to ensure good adhesion of the gold). The glass slides were cleaned by first ultrasonicating them in a mixture of Decon 90 in Millipore Milli-Q water and finally via the use of a plasma cleaner. The slides were then placed directly into the evaporator. The evaporator used was an Edwards Auto 306 Turbo. A vacuum of $<5 \times 10^{-6}$ mbar was used, and 100 Å of chromium was evaporated onto the slides, followed by ∼1500 Å of gold (99.99%). Once prepared, the gold slides were cleaned immediately before use in a plasma cleaning unit and were subsequently rinsed in Millipore water and dried in nitrogen. Monolayers were formed by the spontaneous adsorption of the aromatic alkanethiol onto the clean gold surface, using a 1 mM dichloromethane (Aldrich, HPLC grade) solution for an adsorption period of at least 1 h.[19] On removal from the solution the substrates were immediately rinsed sequentially in dichloromethane and Millipore water and then dried in nitrogen and gave contact angles of 111 ± 2° for advancing and 104 ± 2° for receding.

Synthesis of Thiol-Stabilized Gold Nanoparticles. The synthesis of the gold nanoparticles was performed using the following materials; hydrogen tetrachloroaurate trihydrate, 99.999% (chloroauric acid), sodium borohydride, 98%, tetraoctylammonium bromide, 98%, and toluene, 98% (HPLC grade), all obtained from Aldrich. The aromaticalkane thiol was synthesized via the procedure given in ref 20. Solutions of all the reagents employed in the synthesis were prepared using standard volumetric techniques, and all glassware was cleaned by ultrasonication in a mixture of millipore water and nonionic detergent, followed by plasma cleaning and rinsing in millipore water.

The synthesis was as follows; (step 1) A bright yellow $HAuCl_4 \cdot 3H_2O$(aq) solution (10 mL; 0.0288M) was added to a flask. (step 2) While the solution was being rapidly stirred 20.6 mL of a 0.0358 M $N(C_8H_{17})_4Br$ (toluene) solution was added. On addition a two-layer separation occurred, with a red organic phase on top and a clear/slightly orange aqueous phase on the bottom. (step 3) On complete removal of the color from the aqueous phase, 23.8 mL of a clear colorless aromatic alkanethiol solution (0.0139 M) was added to the organic phase. (step 4) A $NaBH_4$(aq) (8.25 mL; (0.3836 M) solution was then added to the two-phase solution. There was an immediate color change of the organic phase from red to a black/brown color in the flask. The mixture was then left to achieve thermodynamic equilibrium by being left overnight while continually stirring. (step 5) The organic phase was then separated from the aqueous phase and rotovapped down to approximately 10 mL. (step 6) Absolute ethanol (400 mL) was added to the solution. (step 7) This was then placed in a freezer ($T \approx -18$ °C) overnight to aid precipitation. Note, on addition of ethanol, precipitation started immediately. The dark brown/black precipitates were filtered using a 0.26 μm PTFE filter, washed with ethanol, and then dried on a vacuum line. The products are extremely soluble in toluene, hexane, DCM, and chloroform and may be repeatedly precipitated and redissolved, forming faint to dark red solutions, depending on the concentration of the final product used.

The volumetric values given above are those which were used in the formation of gold nanoparticles which had a gold to sulfur ratio of 0.86:1; this corresponds to the formation of gold nanoparticles with the smallest core sizes. To form gold nanoparticles with core sizes of larger dimensions the gold to sulfur ratio has to be increased. Gold colloids (200 Å; mean particle size = 181 Å; standard deviation = 80 Å) were purchased from Sigma.

Transmission Electron Microscopy. Bright field images were obtained using a Philips EM430 TEM operating at 200 kV. The samples were prepared by placing a dilute solution containing the nanoparticles on a carbon-coated copper grid (400 mesh) and allowing the solvent to evaporate. The nanoparticle size distributions were determined via a Kontron Electronik Image Analyser using IBAS software version 2.5.

X-ray Photoelectron Spectroscopy. XPS measurements were made using the Scienta ESCA-300 instrument at Daresbury Laboratories, Warrington, U.K. A monochromatic A1 Kα X-ray source at 1464.6 eV was used. C 1s, O 1s, Au 4f, and S 2p levels were recorded, at an electron take-off angle of 90°. The base pressure in the sample chamber was $<10^{-9}$ mbar. The power level used was 2.8 kW for all samples. The analyzer slit width and pass energy were 1.9 mm and 150 eV, respectively, and the system was calibrated with respect to the Ag 3d peak from a standard sample.

UV/vis Spectroscopy. UV/vis spectra were obtained using a Shimadzu UV-2101PC UV/vis scanning spectrophotometer. Solution spectra were obtained by measuring the absorption of dilute solutions in a quartz cell with a path length of 1 cm. Solid state spectra were obtained by depositing one or two drops of a DCM solution containing the nanoparticles onto the quartz substrate and allowing the DCM to evaporate.

Fourier Transform Infrared Spectroscopy. Grazing angle reflection FTIR spectra were recorded for monolayers on planar surfaces; these were taken at an angle of incidence of 80° using a Bruker IFS-48 spectrometer. Spectra were obtained after purging in dry air for several hours and were background subtracted from the spectrum obtained from a reference sample of freshly cleaned gold. Spectra were taken over 2000 scans at a resolution of 2 cm^{-1}.

Transmission spectra, for the nanoparticles, were obtained by placing one or two drops of a nanoparticle solution onto a calcium fluoride disk and allowing the DCM to evaporate. The spectrum obtained was subtracted from a background spectrum of a clean calcium fluoride disk. Spectra were taken for 2000 scans at a resolution of 2 cm^{-1}.

Bulk crystalline (KBr) spectra of the alkanethiol used were obtained by forming thin (∼100 μm) transparent pellets of the compounds in KBr matrices. Transmission spectra of the pellets were obtained, after purging in dry air, and were background corrected using a reference 'blank' KBr pellet. Spectra were obtained for 200 scans, at a resolution of 2 cm^{-1}.

Results and Discussion

Nanoparticles containing the aromatic surfactant derivatives were formed using the aforementioned process; the ratios of gold/sulfur (thiol) for the reaction mixtures were as follows: 0.86:1, 2.59:1, 3.45:1, and 5.09:1, which correspond to samples I, II, III, and IV. The increasing Au/S ratios should lead to an increase in gold core size. Leff *et al.* estimate that the core diameter (radius) should vary logarithmically with increasing Au/S ratios.

Particle Size Determination by Transmission Electron Microscopy. Bright field TEM micrographs of the thiol-stabilized nanoparticles (Figure 1) show that for samples I−IV the mean diameter is 2−3 nm with a standard deviation of 0.5−0.9 nm, which is in agreement with values found by previous researchers. While the mean diameter stays approximately constant, the form of the distribution of particle sizes does not. Indeed, we find that the highest Au/S ratio gives rise to a "skewed distribution" with a mean diameter of 2−3 nm but with a larger number of nanoparticles with sizes in the range

(17) Puech, K.; Henari, F.; Blau, W.; Duff, D.; Schmid, G. *Europhys. Lett.* **1995**, *32*, 119.

(18) Badia, A.; Gao, W.; Singh, S.; Demers, L.; Cuccia, L.; Reven, L. *Langmuir* **1996**, *12*, 1262.

(19) Caution should be taken with the choice of solvent used, as different solvents behave very differently. Manuscript in preparation.

(20) Evans, S. D.; Urankar, E.; Ulman, A.; Ferris, N. *J. Am. Chem. Soc.* **1991**, *113*, 4123.

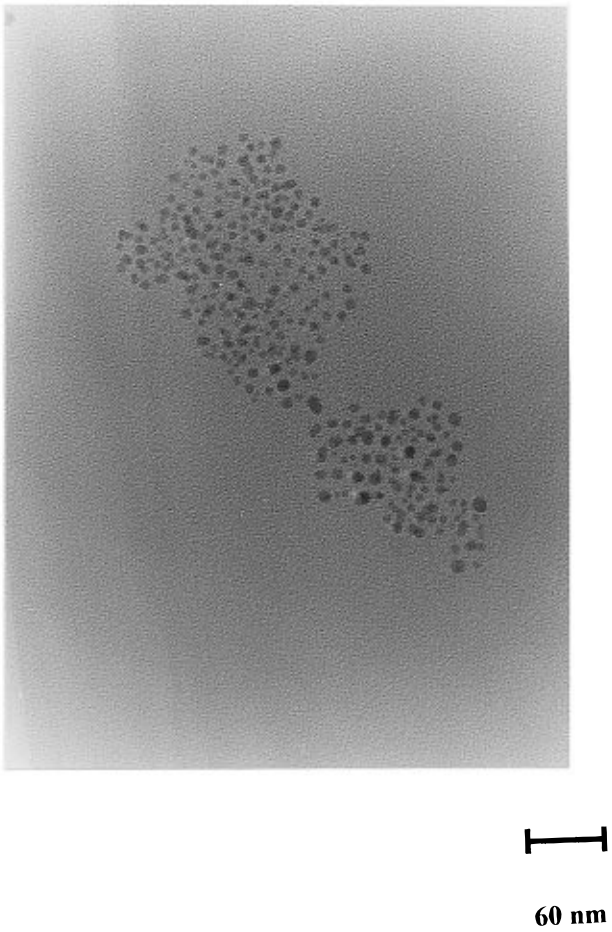

Figure 1. TEM picture of surfactant-stabilized gold nanoparticles from sample I.

4−6 nm. The lower ratios gave a "normal distribution". Thus it appears that while increasing the Au/S ratio does lead to the presence of larger nanoparticles, the distribution is not uniform and suggests there is a low correlation between the core size of the nanoparticles and the initial starting Au/S ratios. At present it is unclear why this should be so; the only significant difference between our systems and those reported by Leff *et al*. is incorporation of the polar aromatic group contained within the alkanethiol chain.

Comparison of our results to the theoretical predictions of Leff *et al*. suggest that our highest Au/S ratios should have a size of ∼20 nm while TEM gives the particle size to be between 2 and 3 nm.

Determination of Nanoparticle Constituents via X-ray Photoelectron Spectroscopy. XPS measurements were made on all nanoparticle samples (I−IV); samples were prepared by placing one or two drops of a dichloromethane solution of nanoparticles onto a clean Si substrate and allowing the solvent to evaporate.

The XPS spectra show the presence of both the Au and the alkanethiol material. Elemental analysis showed that there was no evidence of the starting materials. The alkanethiol molecule contains C, S, and O species, present in several different forms; nanoparticles formed with different Au/S ratios were all similar, and only the spectra for the nanoparticles formed from the Au/S ratio 0.86:1 are described in detail.

The C 1s region (Figure 2), contains two bands at 284.9 ± 0.2 eV and 286.5 ± 0.2 eV; the band at 284.9 eV corresponds to *C*−*C* bonded atoms and compares well with the characteristic carbon peak at 284.7 eV, while the band at 286.5 eV is due to the contributions from the *C*−O

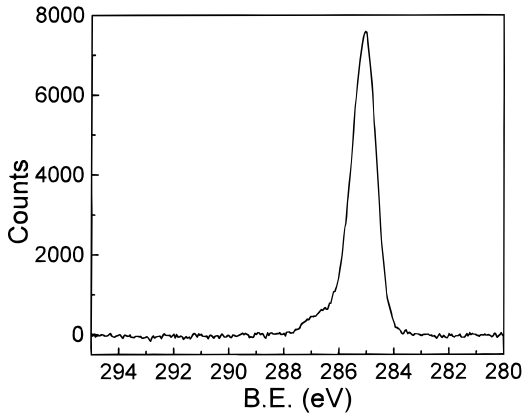

Figure 2. XPS spectra of the carbon 1s region, for particles of sample IV.

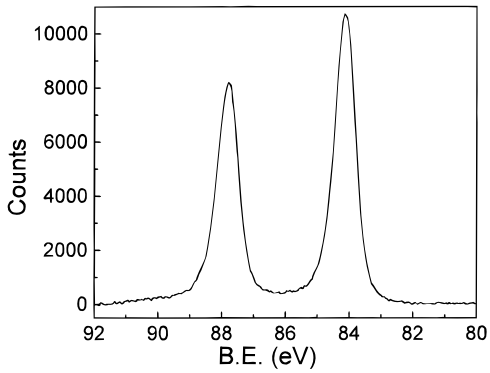

Figure 3. XPS spectra of the gold $4f_{7/2}$ and $4f_{5/2}$ region, for particles of sample IV.

bond.[21,22] The ratio of the area of the lower binding energy component to that at higher binding energy, obtained for each of the nanoparticle groups, gives a value of ∼7, while the value expected on the basis of on the molecular structure gives a value of 8.

The O 1s band appeared to be a composite of two or more peaks. Curve fitting this band, to two peaks, gave peak positions at 532.2 ± 0.2 eV and 533.1 ± 0.2 eV, respectively.[23] The band occurring at 533.1 eV is attributed to the oxygen atoms present in the ether links, i.e. C−*O*−C, while the band at 532.2 eV is ascribed to oxygen atoms contained within the SO_2 species, present in the 'upper' alkyl chain portion of the molecule.

The S 2p spectra gave only weak signals due to the small scattering cross-section of the S and the low amount of material present. This region has two doublets (S $2p_{3/2}$, S $2p_{1/2}$) at 162.4 ± 0.2 eV and 163.5 ± 0.2 eV respectively, for the thiolate and 168.0 ± 0.2 eV and 169.3 ± 0.2 eV for the sulfone.[24] The spectra for the C, O, S regions are all consistent with the presence of the thiol used within this study.

Figure 3 shows a spectrum of the Au 4f region, two gold bands $4f_{7/2}$ and $4f_{5/2}$, which occur at 84.3 ± 0.2 eV and 87.9 ± 0.2 eV respectively. While there is a slight difference in the peak positions present here and those given by Brust *et al*., the differences between the two peaks are the same (3.7 eV), and our peak positions are also similar in

(21) Bain, C. D.; Troughton, E. B.; Tao, Y.-T.; Evall, J.; Whitesides, G. M.; Nuzzo, R. G. *J. Am. Chem. Soc.* **1989**, *111*, 321.
(22) Beamson, G.; Briggs, D. *High Resolution XPS of Organic Polymers*; John Wiley & Sons: Chichester, U.K., 1992.
(23) Evans, S. D.; Ulman, A.; Goppert-Berarducci, K. E.; Gerenser, L. J. *J. Am. Chem. Soc.* **1991**, *113*, 5867.
(24) Evans, S. D.; Goppert-Berarducci, K. E.; Urankar, E.; Gerenser, L. J.; Ulman, A.; Snyder, R. G. *Langmuir* **1991**, *7*, 2700.

Table 1. Positions of the Binding Energy Peaks of the Various Regions Investigated via XPS

	binding energy positions (eV)									
	Au									
sample	$4f_{5/2}$	$4f_{7/2}$	C 1s		O 1s		S 2p			
I	87.8	84.1	285.1	286.3	532.2	533.5	162.3	163.6	168	169.1
II	88	84.4	284.9	286.4	532.3	533.7	162.1	163.3	167.9	169
III	88	84.3	285	286.1	532.5	533.6	162.4	163.7	168	169.2
IV	88	84.3	284.9	286.5	532.2	533.3	162.4	163.7	167.8	169
ODT	87.6	83.9	284.7				162.1	163.3		

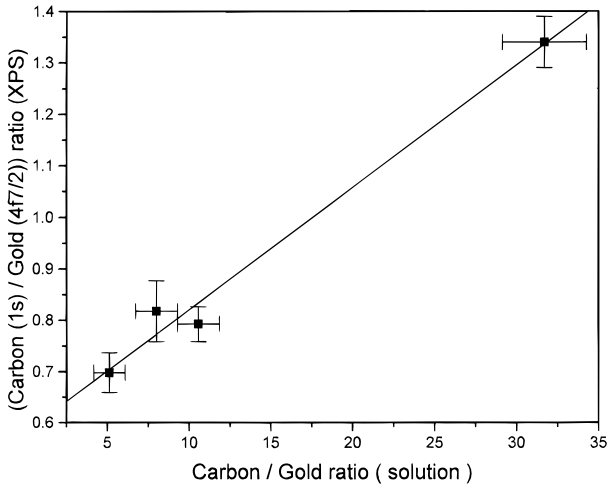

Figure 4. (C 1s/Au $4f_{7/2}$) ratio, from XPS data, as a function of the C/Au ratio present during the synthesis.

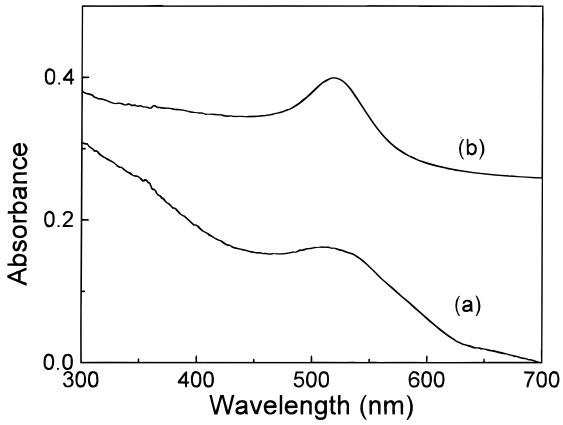

Figure 5. Comparison between the UV/vis spectra of (a) a surfactant-stabilized gold nanoparticle (sample IV) and (b) a 20 nm gold colloid.

position to those obtained from bulk evaporated gold.[25] Due to higher resolution in our spectra in comparison to the one given by Brust *et al.*, we note that there is little, if any, evidence of oxidation of the gold.[26] On thiolate formation one would expect a significant proportion of the outer gold atoms to be oxidized from Au^0 to Au^1. Such an oxidation is expected to give a contribution to the Au $4f_{7/2}$ peak shifted to 84.9 eV, i.e. to higher binding energies, by 0.6 eV.[27] Our results suggest that the majority of the gold atoms in the clusters must be in the Au^0 state. There is some variation in peak positions, which is due to surface charging effects. However according to Schon *et al.* the number of gold atoms in the gold cores of the nanoparticles follow a set of magic numbers depending on the packing of the atoms used.[28] For an average diameter of 2.5 nm, one would expect the number of gold atoms in the core to be 309 or 409, depending on whether one considers the core to be a perfect sphere or a cubooctahedral; therefore, there are 162 or 191 gold atoms which make up the surfaces of the clusters. This would imply that between 1/3 and 1/2 of the Au atoms should be present in the Au^1 state. There appears to be no strong evidence for this.

Table 1 gives a summary of the peak positions found for the nanoparticles. Comparison of the spectra from a planar gold substrate with those from a nanoparticle sample shows essentially identical spectra. In both cases the full width at half maxima (fwhm's) of the planar gold substrate and the nanoparticles, 0.51 ± 0.03 and 0.7 ± 0.03 eV, respectively, are similar and indicate that the Au is largely in the Au^0 oxidation state.

Figure 4 shows the C/Au ratio for samples I−IV (obtained from XPS measurements) plotted against the corresponding ratio of C (thiol)/Au used in the initial synthesis solution. The scale ranges from 1:1 to 32:1, which takes into account that there are 32 carbon atoms for each thiol sulfur atom present in the initial synthesis. There appears to be an approximately linear relation between these, which suggests that the distribution of particle sizes must be changing even though the mean size is approximately constant.

Investigation of Nanoparticle Structure via UV/vis Spectroscopy. The absorption spectra of the nanoparticles in solution and on quartz slides were observed using a UV/vis scanning spectrophotometer.

Nanoparticles in Solution. All samples gave spectra which show a continuous rising background, towards higher energies, which is due to Mie scattering from the nanoparticle solution.[29] Superimposed on the background, between 500−550 nm, is a peak corresponding to a surface plasmon polariton generated within the gold nanoparticles (Figure 5).[30] The coupling to the plasmon mode is sensitive to the refractive index of the surrounding solvent. This was not investigated in detail here but has been widely acknowledged in general.[31] The peak positions and integration of the plasmon absorption were calculated from the spectra as a function of concentration. Figure 6 shows that the integrated intensity of this absorption increases linearly with increasing concentration of nanoparticles. The position for the maxima remains approximately fixed for all nanoparticle mixtures; i.e., it does not appear to vary significantly as a function of core diameter. This lack of concentration dependence indicates that there is no significant aggregation of particles within the solution. We attribute this to a combination of the size of the ligand shell (≈25 Å), preventing gold clusters from getting closer than 50 Å, and the weak attractive interactions between

(25) Evans, S. In *Handbook of X-ray and Ultraviolet Photoelectron Spectroscopy;* D. Briggs, Ed.; Heyden & Son: London, 1977; Chapter 3.
(26) King, D. E. *J. Vac. Sci. Technol., A* **1995**, *13* (3), 1247.
(27) McNeillie, A.; Brown, D. H.; Ewen Smith, W. *J. Chem. Soc., Dalton Trans.* **1980**, 767.
(28) Schon, G.; Simon, U. *Colloid Polym. Sci.* **1995**, *273*, 101−117.
(29) Creighton, J. A.; Eadon, D. G. *J. Chem. Soc., Faraday. Trans.* **1991**, *87*, 3881.
(30) Mulvaney, P. *Langmuir* **1996**, *12*, 788.
(31) Underwood, S.; Mulvaney, P. *Langmuir* **1994**, *10*, 3427.

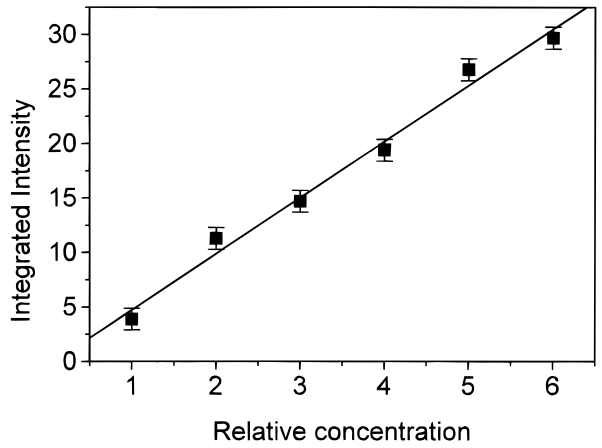

Figure 6. Graph to show how the integrated intensity of the plasmon peak varies as a function of concentration for gold nanoparticles in solution.

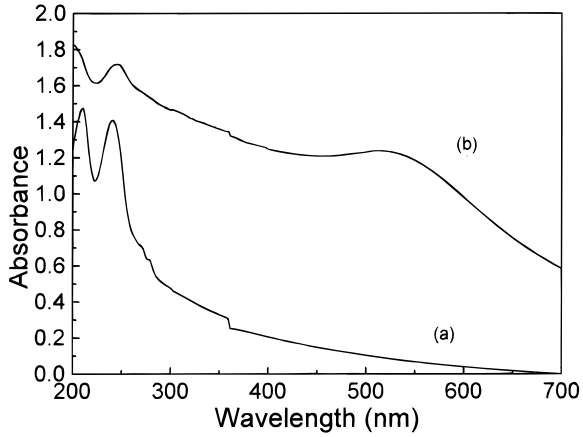

Figure 7. Comparison between the UV/vis spectra of (a) a thin film on quartz of the thiol used in the synthesis of the gold nanoparticles and (b) a thin film on quartz of the gold nanoparticles.

Table 2. Positions of the Secondary Peaks of a Thin Gold Film of Gold Nanoparticles on Quartz

sample	peak 1 (nm)	peak 2 (nm)
I	203.3	242.1
II	198.2	242.9
III	200.9	242.1
IV	197.7	242.9

the nanoparticles.[32] The intensity of the plasmon peak for bare gold colloids (Figure 5 b), having a core diameter of 200 Å, is much greater than that of the surfactant-stabilized gold nanoparticles, which have a gold core of diameter 25 Å. This could be due to a damping effect on the plasmon polariton band by the aromatic alkanethiol or due the fact that surfactant-stabilized nanoparticles are of insufficient size to efficiently couple to the plasmon polartion.

Nanoparticles as a Cast Film on a Quartz Substrate. For nanoparticles deposited onto quartz substrates, one is also able to observe an additional absorption due to the chromophore. Figure 7b shows the spectra obtained from the nanoparticles, while Figure 7a shows that obtained from a cast film of the thiol material on quartz. The peaks associated with the chromophore occur at shorter wavelengths, $\lambda = 205$ and 250 nm, in the ultraviolet region of the spectra.

The plasmon peak, occurring at 540 nm, is red shifted with respect to those of solution spectra. This is attributed

(32) Changing the terminal group can be used to significantly alter the physical properties. Unpublished results.

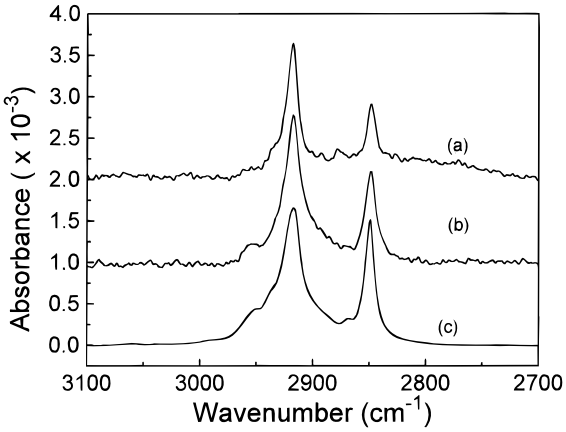

Figure 8. Comparison of the "high-frequency region" for (a) a monolayer of the thiol on planar gold, (b) a KBr pellet of the thiol, (c) and a monolayer of the thiol on the surface of a gold nanoparticle.

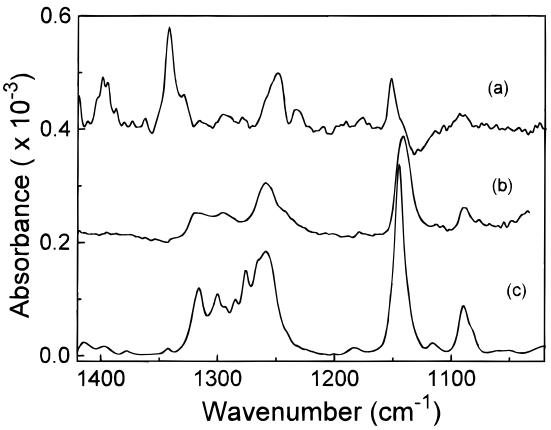

Figure 9. Comparison of the "midfrequency region" for (a) a monolayer of the thiol on planar gold, (b) a KBr pellet of the thiol, (c) and a monolayer of the thiol on the surface of a gold nanoparticle.

to a decrease in the average particle separation resulting in cooperative modes.[33] Investigation of the absorption peaks associated with the thiol derivative shows that the shortest wavelength peak (205 nm) in the nanoparticle spectra varies its position as a function of particle distribution (Table 2). This peak could possibly be reflecting changes in the chromophore density or packing.

Conformation and Composition Investigated via Fourier Transform Infrared Spectroscopy. FTIR yields information regarding both the composition and the molecular conformation of the ligand-stabilizing 'thiol derivatives' surrounding the metallic cores. For comparative purposes we present the spectra obtained both from ligand stabilized nanoparticles and for SAMs formed on planar substrates (we also include spectra of the pure thiol derivative obtained in the form of a KBr pellet).

The spectra of the so-called "high-frequency" and "midfrequency" regions are shown in Figures 8 and 9. The "high-frequency" region contains spectral contributions from the CH_2 and CH_3 symmetric (υ_s) and asymmetric (υ_{as}) vibrations. The peak positions and full width half at maximum values (see Table 3), give information regarding the conformational order for the thiol derivatives in their different molecular environments. In all cases, i.e. for planar monolayers (curve a), nanoparticles (curve c), and KBr pellets of the alkanethiol derivative (curve b), the peak positions of the CH_2 υ_s and CH_2 υ_{as} stretches occur

(33) Itakura, T.; Toriggoe, K.; Esumi, K. *Langmuir* **1995**, *11*, 4129.

Table 3. Labeling of All the Stretches Associated with the Thiol Molecule, as a Monolayer on Planar Gold, a Monolayer on the Surface of a Gold Nanoparticle, and KBr Pellet

peaks	KBr pellet	monolayer position (FWHM) cm^{-1}	nanoparticle
CH_2 υs	2850(9)	2849(8)	2849(11)
CH_3 υs	2869(5)	2879(8)	2870(4)
CH_2 υas	2917(17)	2918(11)	2918(18)
CH_3 υas	2950(8)	2953c	2955(11)
C═C skeletal stretch[a]	1598(9)	1599(8)	1595(10)
C═C skeletal stretch[b]	1578(5)	1576(3)	1577(6)
C═C skeletal stretch[a]	1501(8)	1501c	1497(9)
C═C skeletal stretch[b]	1469(10)	1471c	1467(3)
SO_2 υ_{as}	1316(9)	1340(10)	1318(9)
C−O−C υ_s	1259(16)	1249(16)	1257(21)
SO_2 υ_s	1145(10)	1152(9)	1140(15)
in plane phenyl bend	1090(12)	1089(6)	1089(9)

[a] Parallel to the molecular axis. [b] Perpendicular to the molecular axis. [c] Full width at half maxima were not resolvable in these spectra.

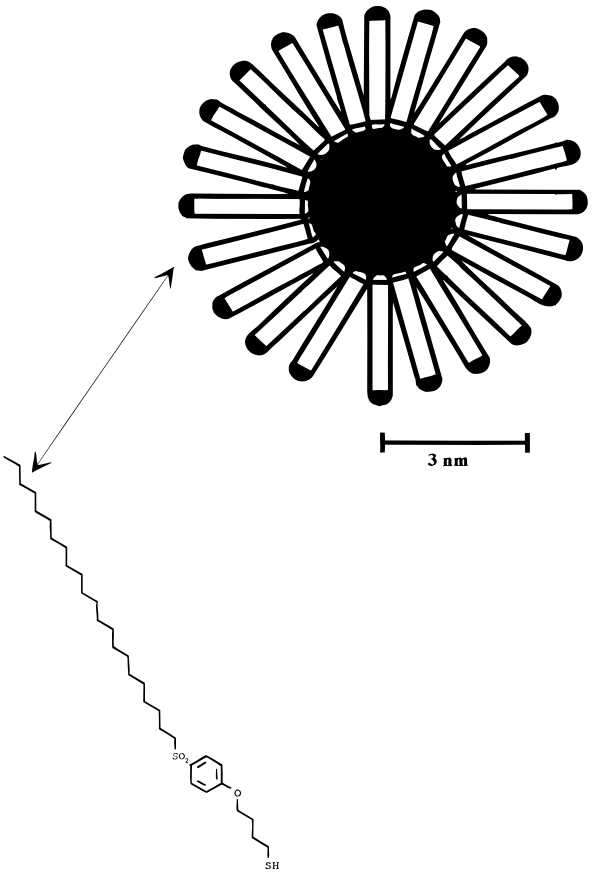

Figure 10. Cartoon representation of a thiol-capped gold nanoparticle (to scale) to show the free volume available for conformation changes or interparticle penetration. Also included is the chemical structure for the thiol ($C_{22}H_{25}-SO_2-C_6H_4-O-(CH_2)_4-SH$).

at 2848 cm^{-1} and 2918 ± 2 cm^{-1}, respectively. Such 'low' wavenumber values for these stretches indicate that the SAM is in an 'ordered' environment and that the degree of conformational disorder appears to be low; this is somewhat surprising, due to the free volume expected for the adsorption onto such a highly curved surface (Figure 10). one possible explanation is that there may be interpenetration of chains from adjacent particles, leading to a denser hydrocarbon region toward the end of each alkyl chain.[18,34] It should be noted that the results presented here were obtained using transmission geometry for curves b and c and reflectance geometry for curve (a). The FWHM values obtained for the planar monolayer are significantly smaller than those obtained for the coated nanoparticles and for the KBr pellet of the pure thiol. The later observation may be indicative of some differences in conformational order or may be indicative of the different molecular environment of the thiol molecules. The fwhm values are still within the range of values considered to be indicative of systems containing low proportions of conformational defects.[35,36] Also the peak positions of the CH_2 ν_s and CH_2 ν_{as} for the SAMs on the nanoparticles are in excellent agreement with the results of Lennox *et al.* for a C_{18} monolayer and of Hostetler *et al.* for a C_{24} monolayer. The values for the fwhm's are also similar to those reported, except in the case of the CH_2 ν_{as} where Hostetler *et al.* find the fwhm to be much broader (similar to the values typically quoted for liquid-like alkanes).

The "midfrequency" region (Figure 9) contains a wealth of spectral information regarding the chemical composition of alkanethiol derivative. Curves a, b, and c correspond to a planar monolayer, KBr, and nanoparticle samples, respectively. Between 1450 and 1650 cm^{-1} (not shown) are four peaks associated with the para-substituted phenyl ring.[13,37] The vibrations at 1595 and 1498 cm^{-1} are associated with the a_1 modes parallel to donor-acceptor substitution across the ring. The peaks at 1595 and 1498 cm^{-1} are associated with the b_2 modes which are perpendicular to the ring. These phenyl peaks are well documented, and their relative intensities vary with the degree of coupling between the donor and acceptor groups across the ring. The peak at ~1400 cm^{-1} in the planar monolayer spectra is absent in both the KBr and nanoparticle spectra. We believe that this peak is due to the structure within the planar SAM; however, it is unclear at present why this peak is absent from the other two systems.

The strong band near 1340 cm^{-1} in the monolayer spectra (Figure 9a) is attributed to the SO_2 asymmetric stretching mode; this band appears to be split with a second component lying to slightly lower wavenumber (ca. 1330 cm^{-1}). The corresponding symmetric stretch occurs at 1152 cm^{-1}. The nanoparticle and KBr spectra (curves b and c) are similar to each other but show marked differences from that of the planar SAM. In particular the asymmetric SO_2 peak(s) is now much weaker and appears to be shifted to much lower wavenumbers (~1316 cm^{-1}). The ratio of the relative intensities of the symmetric to asymmetric stretches have changed from ~0.5 (planar monolayer) to ~4 (nanoparticle); this may be attributed to be due to the surface selection rule which is in operation for the case of monolayers on planar substrates but not for the nanoparticle samples.[38]

The fwhm of the SO_2 ν_s stretch for nanoparticle samples is significantly larger, ~15 cm^{-1}, than those obtained from the monolayer and KBr samples, ~10 cm^{-1}, possibly suggesting a decrease in the conformational order in the central portion of the molecule (close to the SO_2 group). The aryl oxygen stretch, below the ring, has a characteristic frequency close to 1260 cm^{-1} for the KBr pellet and nanoparticles and 1250 cm^{-1} for the planar SAM. The KBr spectra also show the presence of the wagging vibrations, due to the alkyl chain, between and overlapping with the C−*O*−C and SO_2 ν_{as} stretches.

(34) Ulman, A. *An Introduction to Ultrathin Organic Films*; Academic Press: San Diego, CA, 1991.
(35) Gao, W.; Reven, L. *Langmuir* **1995**, *11*, 1860.
(36) Porter, M. D.; Bright, T. B.; Allara, D. L.; Chidsey, C. E. D. *J. Am. Chem. Soc.* **1987**, *109*, 3559.
(37) Jackobsen, R. J.; Brewer, E. J. *Appl. Spectrosc.* **1962**, *16*, 3.
(38) Greenler, R. G. *J. Chem. Phys.* **1966**, *44*, 310.

In general the IR spectra for the alkanethiol-derivatized nanoparticles are similar to those obtained from KBr pellets, as opposed to those obtained from SAMs adsorbed on a planar gold substrate. Therefore it appears that the IR beam is incident upon a random distribution of thiol-derivatized gold nanoparticles and that the surface selection rule for SAMs on planar gold substrates is not applicable in the case of nanoparticles.

Conclusions

Numerous experimental techniques have been used to establish the formation of ligand-stabilized gold nanoparticles. By using $C_{22}H_{45}-SO_2-C_6H_4-O-C_4H_8-SH$, we have shown that it is possible to incorporate chromophores containing large dipole moments, essentially perpendicular to the surface, into the stabilizing monolayer. The long term relevance of this is in manipulating the electronic properties of the metallic core and in controlling the sphere−sphere interactions.

The nanoparticles contain a gold core ~25 Å in diameter surrounded by a sheath of the alkanethiol derivative. The core size was determined by TEM, and the core content, by XPS, which also showed the characteristic gold $4f_{5/2}$ and $4f_{7/2}$ peaks. The CH_3 terminal groups, at the particle/ambient interface, lead to relatively weak sphere−sphere interactions and permit the solubilization of the nanoparticles into organic solvents. Somewhat surprisingly we found only relatively weak dependence effects between nanoparticle size and the initial Au/S ratio. The reason for this is unclear at present. The UV/vis results showed the presence of the plasmon polariton band whose position, was independent of the sample state, i.e. solution concentration or as a solid film, indicating that the properties observed are 'single' particle properties. The infrared studies show that the spheres are indeed coated with the alkanethiol moiety and possibly that the overlayer contains a greater number of conformational defects than SAMs formed on planar surfaces.

Acknowledgment. We wish to acknowledge Dr. A. Marsh from the University of Warwick for his advice on the synthesis of the nanoparticles. One of us (S.R.J.) would like to acknowledge receipt of a Departmental Scholarship. This work was carried out in the Centre for Self Organising Molecular Systems at Leeds University.

LA9607520